Turk J Elec Eng & Comp Sci, Vol.17, No.3, 2009, © TÜBİTAK
doi:10.3906/elk-0908-166

Variance and kurtosis-based characterization of resonances in stochastic transmission lines: local versus global random geometries

Ousmane Oumar SY[1], **Martijn C. van BEURDEN**[1]
Bastiaan L. MICHIELSEN[2], **Antonius G. TIJHUIS**[1]
[1]*Electromagnetics Group, Department of Electrical Engineering, Eindhoven University of Technology*
Den Dolech 2, 5600 MB, Eindhoven, THE NETHERLANDS
e-mail: O.O.Sy@tue.nl, M.C.v.Beurden@tue.nl, A.G.Tijhuis@tue.nl
[2]*ONERA - DEMR, BP 74025, 2, av. Edouard Belin, 31055 Toulouse Cedex 4, FRANCE*
e-mail: Bastiaan.Michielsen@onera.fr

Abstract

A stochastic method is proposed to characterize electromagnetic couplings involving geometrically perturbed transmission lines. A combined exploitation of suitably defined statistical tools is presented to appreciate the intensity of the dispersion of response variables both physically via the variance, and statistically through the kurtosis or fourth-order moment. The usefulness of this method to analyze resonances is illustrated by the study of a transmission line affected by two different types of random geometrical perturbations, viz. a local deformation modeled by a wavelet and global sinusoidal undulations.

1. Introduction

Numerical methods are a precious help in ElectroMagnetic Compatibility to represent electromagnetic interactions between material objects, and electromagnetic fields incident on them. Compared to experiments, they constitute an economical means of investigating a variety of coupling configurations, as can be needed for the analysis of performance and the consequences of fatigue and ageing studies.

The accuracy of the response quantities of these modes, also known as "observables", depends on the accuracy of the characterization of the interaction configuration. In reality, many practical cases arise where such knowledge cannot be guaranteed due to changing operational conditions, ageing, or a prohibitive complexity. The effect of uncertainties in the configuration should hence be accounted for, to highlight the limits of the model and to improve on the pertinence of its predictions.

Among the existing uncertainty quantification methods, a systematic study of all the possible configurations yields an exhaustive picture of the electromagnetic coupling, but it can be numerically intractable due to the large amount of computations required. Conversely, a sensitivity analysis based on the study of a few configurations will generally be very efficient numerically, but it will provide only local information about the behavior

of the observable. From these perspectives, a stochastic approach represents an interesting alternative to both of the aforementioned quantification methods: it uses probability theory to handle the global fluctuations of the configuration and to characterize the variations of the observable via a smaller number of calculations than an exhaustive deterministic approach.

Owing to these interesting features, stochastic methods are often employed to study the field distribution in a mode-stirred chamber [10, 7, 8]. The propagation of signals in complex surroundings such as urban areas is also often handled stochastically, in particular to take the multipath phenomena into account [5, 3]. Stochastic methods are also employed to investigate the electromagnetic properties of wire structures that are present for instance in medical, aeronautical or military devices. The underlying deterministic model is based either on transmission-line theory [16, 2], which provides analytical solutions for the electromagnetic observables such as the induced voltage or the current at some port of the device, or based on a thin-wire integral equation which is solved numerically. We have applied the latter approach to study the voltage V_e, induced by a plane wave incident on a randomly undulating frame. The quality of the quantification achieved by evaluating and interpreting the average and the variance has been illustrated in [20, 21] and confirmed experimentally in [22]. However, the variance alone provides only a general idea of the spread of V_e around its average, whereas in sensitive medical automotive or aeronautical devices, the assessment of the risk posed by extreme values of V_e, caused for instance by resonances, also calls for special attention. As shown in [23, 24], the detection of such a risk amid a large set of samples of V_e is feasible through the calculation of the fourth-order moment, or kurtosis, of V_e. The present paper is an extension of the aforementioned contributions as it employs the variance and the kurtosis to compare the behavior of thin-wire structures affected either by localized geometrical perturbations as in [24], or by global fluctuations as in [23].

In Section 2 a deterministic interaction model is presented, which provides the Thévenin voltage V_e induced at the port of a thin wire illuminated by an incident field. The subsequent randomization of this model in Section 3 permits the definition of the average, the variance and the kurtosis of V_e, which can be computed by quadrature. The valuable information conveyed by these moments is then illustrated in Section 4 for the case of a thin wire affected by local wavelet-type deformations that are randomly located and secondly through the example of a wire undergoing global sinusoidal undulations of random amplitude. Comparisons between the two different types of setups will then highlight some commonalities, particularly concerning the efficiency of the kurtosis to identify risky frequencies around resonances, unlike the variance.

2. Deterministic interaction

The setup studied in this paper is first described in a deterministic context, i.e. when all the parameters defining the configuration of the electromagnetic coupling are known. In the present case, a perfectly electrically conducting (PEC) thin-wire frame is considered. This wire, denoted S and depicted in Figure 1, comprises two 5 cm long vertical wires, one of which contains a port region. These poles are connected below to an infinite ground plane and above by a thin wire parameterized by its Cartesian coordinates $(x = 0, y, z = h(y))$. The smooth function h can consist of a sum of sines, in agreement with the mechanical mode representation of a vibrating string. Alternatively, h may be given in terms of wavelets which allow for a multi-resolution geometrical model.

The effect of external sources is expressed by the incident field $\boldsymbol{E}^i$, which induces a voltage V_e at the port of

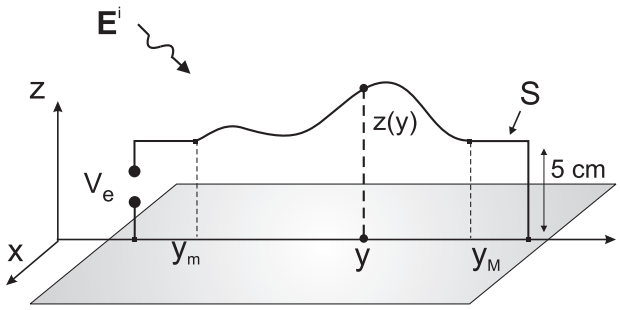

Figure 1. Interaction configuration.

S. This voltage reads [15, 25]

$$V_e = -\frac{1}{I_T} \int_S \boldsymbol{j} \cdot \boldsymbol{E}^i, \tag{1}$$

where the transmitting-state current $\boldsymbol{j}$ is induced on S in the absence of $\boldsymbol{E}^i$, when a current source I_T is impressed at the port. The current $\boldsymbol{j}$ is calculated by solving, via the method of moments, a frequency-domain electric-field integral equation (EFIE) modeling the transmitting state [25]. Such a model bears a certain cost stemming from the need to fill a full impedance matrix and to solve the subsequent linear system. This numerical cost is optimized by using quadratic-segment basis functions [4], together with a reduced kernel in Pocklington's thin-wire integral equation [14].

Moreover, resonances will appear at frequencies where a wave, propagating along the waveguide formed by the wire and the ground plane, becomes resonant due to the boundary conditions at the wire extremals.

This test-case, derived from an EMC benchmark [17], stands for a large class of interaction problems, for example the common-mode interference appearing at the connection of a power cable to a printed circuit board or certain types of wire antenna problems. An example of practical application involving such a setup can be found in [19], where the wire represents cables that connect a control computer of a helicopter to the rotor actuators. Automotive examples are analyzed in [1, 6] where the immunity of a car wiring to external sources of perturbation, such as GSM or bluetooth, is investigated.

3. Stochastic rationale

3.1. Randomization

The parameters of the deterministic model presented above may be hindered by uncertainties concerning the geometry of the device S. A stochastic quantification of the aforementioned uncertainties starts by regarding the uncertain parameters as random variables within their ranges. As a preliminary step, all the uncertain input parameters are gathered in the vector $\boldsymbol{u} = (u_1, \ldots, u_d) \in \mathcal{U} \subset \mathbb{R}^d$. The cornerstone of the stochastic method

resides in the assumption that $\boldsymbol{u}$ is randomly distributed in $\mathcal{U}$ according to an a priori *known* probability distribution $P_{\boldsymbol{u}}$, or equivalently a known probability density function (pdf) $f_{\boldsymbol{u}}$. Establishing $f_{\boldsymbol{u}}$ can, for instance, be guided by the exploitation of manufacturing data-sheets, when available, from experiments or from physical considerations.

The randomness of the parameters $\boldsymbol{u}$ of the configuration induces in turn the randomness of V_e. To mark this dependence, V_e is written as $V_e(\boldsymbol{u})$. A complete characterization of the randomness of $V_e(\boldsymbol{u})$ is only possible by identifying its probability distribution P_{V_e}, which can be expressed in terms of $P_{\boldsymbol{u}}$ as [18]

$$P_{V_e} : \mathbb{C} \ni v' \longmapsto P_{\boldsymbol{u}}\left(V_e^{-1}(v')\right) \in \mathbb{R}_+. \tag{2}$$

The latter equation is however not directly usable in practice owing to the intricate dependance of V_e on $\boldsymbol{u}$ via an integral equation, which severely complicates the determination of the reciprocal function V_e^{-1}.

Unlike P_{V_e}, the statistical moments of V_e can be computed and post-processed to obtain partial information about the dispersion of V_e. These statistical moments are obtained by considering a measurable function l acting on V_e and by evaluating the expectation of the random variable $l(V_e)$ as follows

$$\mathbb{E}[l(V_e)] \quad = \quad \int_{\mathcal{U}} l(V_e(\boldsymbol{u}'))f_{\boldsymbol{u}}(\boldsymbol{u}')d\boldsymbol{u}'. \tag{3}$$

The integral in this equation is defined over the known domain $\mathcal{U}$ and has an integrand that consists of computable terms, viz $l(V_e(\boldsymbol{u}'))f_{\boldsymbol{u}}(\boldsymbol{u}')$. Equation (3) can therefore be approximated by a quadrature rule as follows

$$\mathbb{E}[l(V_e)] \quad \approx \quad \sum_{k=1}^{N} l(V_e(\boldsymbol{u}_k))f_{\boldsymbol{u}}(\boldsymbol{u}_k)\omega_k, \tag{4}$$

where the abscissae $\boldsymbol{u}_k$ belong to $\mathcal{U}$, the weights ω_k are positive for stable quadrature rules [11, 9] and the number N indicates the complexity as it also corresponds to the number of evaluations of V_e required. This quadrature rule needs to be selected cautiously to efficiently handle the generally multidimensional domain $\mathcal{U}$.

3.2. Physical and statistical dispersions: variance and kurtosis

The mean $\mu[V_e] = \mathbb{E}[V_e]$ and the standard deviation $\sigma[V_e] = \sqrt{\mathbb{E}\left[|V_e - \mu[V_e]|^2\right]}$ are statistical moments that have the same physical dimension as V_e. These "physical" moments quantify the spread of V_e locally around $\mu[V_e]$ as confirmed by Chebychev's inequality [18], which states that

$$P_{V_e}\left(|V_e - \mu[V_e]| > m\sigma[V_e]\right) \leq \frac{1}{m^2}, \text{ for } m \geq 1. \tag{5}$$

The strength of this inequality resides in its validity for all probability distributions that have finite variances. Based on Eq. (5), confidence domains can be defined as disks C_m centered around $\mu[V_e]$ with a radius equal to $m\sigma[V_e]$. Chebychev's inequality then guarantees, for instance, that the measure of the interior of the circle C_2 (resp. C_4) is at least 75% (resp. 93%). These bounds can be too coarse, with a Gaussian distribution, for example, 95% of the values lie C_2.

In physical terms, the dispersion of V_e is measured in Volts via the value of $\sigma[V_e]$. Nonetheless, the magnitude of $\sigma[V_e]$ does not inform about the presence of a extreme values of V_e, lying several $\sigma[V_e]$ away from $\mu[V_e]$. Although Chebychev's inequality ascertains that such extreme values of V_e do not occur frequently, whenever they do occur they can damage electronic devices. Therefore, in practice, improbable is not synonymous with innocuous.

only exceptionally, they can prove for in practice.

These extreme samples are better highlighted by normalizing V_e as follows

$$V_n = \frac{V_e - \mu[V_e]}{\sigma[V_e]}, \quad \text{where } \mathbb{E}[V_n] = 0,\ \sigma[V_n] = 1. \tag{6}$$

Extreme samples of V_e will therefore be such that $|V_n|$ takes a large value. This observation motivates the introduction of the kurtosis of V_e which reads

$$\kappa[V_e] = \mathbb{E}\left[|V_n|^4\right] = \mathbb{E}\left[\left|\frac{V_e - \mu[V_e]}{\sigma[V_e]}\right|^4\right] \geq 0. \tag{7}$$

Since the kurtosis is a fourth-order moment, it weighs the tail of $p_{|V_n|}$ [18, 13] by allocating an important "mass" to very large values of $|V_n|$. Hence, as $\kappa[V_e]$ increases, the likelihood of observing large values of $|V_n|$ grows accordingly.

It is worth noting that the detection of risky values of V_e can also be performed by studying the kurtosis of $|V_e|$, as is done in [23, 24]. The risk indicator $\kappa[|V_e|]$ would then be given by

$$\kappa[|V_e|] = \mathbb{E}\left[\left(\frac{|V_e| - \mathbb{E}[|V_e|]}{\sigma[|V_e|]}\right)^4\right] \geq 0, \tag{8}$$

where $\mathbb{E}[|V_e|]$ and $\sigma[|V_e|]$ come into play instead of $\mu[V_e]$ and $\sigma[V_e]$. In the cases where $\mathbb{E}[|V_e|]$ is close to 0, employing $\kappa[|V_e|]$ or $\kappa[V_e]$ leads to equivalent results since extreme values of V_e will necessarily give rise to extreme values of $|V_e|$ and vice versa.

A joint analysis of the standard deviation and the kurtosis enables the assessment of the distribution of V_e in the entire complex plane: $\sigma[V_e]$ will measure the importance of the spread of V_e around $\mu[V_e]$ in volts, while $\kappa[V_e]$ will quantify the statistical dispersion of V_e by indicating the plausibility of observing some samples of V_e several $\sigma[V_e]$ away from $\mu[V_e]$.

4. Results

4.1. Test-cases

The stochastic method proposed in the previous section is now applied to two different types of thin-wire structures.

First, a wire S_w affected by a local deformation consisting of a so-called Mexican-hat wavelet [12] is considered. With reference to the notations of Section 2, the height of the axis of S_w is given by the function

$$S_w: \quad h_1(y) = 5 + w(y - y_*) \quad \text{in cm} \tag{9}$$

where

$$w(t) = \delta_z \left(\left(\frac{t}{\tau} \right)^2 - 1 \right) \exp \left(- \left(\frac{t}{\tau} \right)^2 \right), \tau = 10 \text{ cm}. \tag{10}$$

The resulting deformation is centered around y_* and spans the range $[y_* - \delta_y/2; y_* + \delta_y/2]$ with $\delta_y \approx 4$ cm, and its amplitude is given by $\delta_z = 4$ cm. The location y_* of the geometrical deformation is assumed to be random and uniformly distributed between the abscissae $[y_m, y_M] = [0.1; 0.9]$ m. The random input of this problem is hence $u = y_* \in [y_m, y_M] = \mathcal{U}$. Figure 4.1 shows some examples of geometries produced by such a parametrization.

In a second stage, a thin wire S_h obtained via harmonic undulations is studied with an axis given by

$$S_h : \quad h_2(y) = 5 + \delta_z \sin(2\pi y) \quad \text{in cm}. \tag{11}$$

In this case the amplitude $u = \delta_z$ is assumed to be random and uniformly distributed in $\mathcal{U} = [-4; 4]$ cm. Figure 4.1 illustrates this type of geometry.

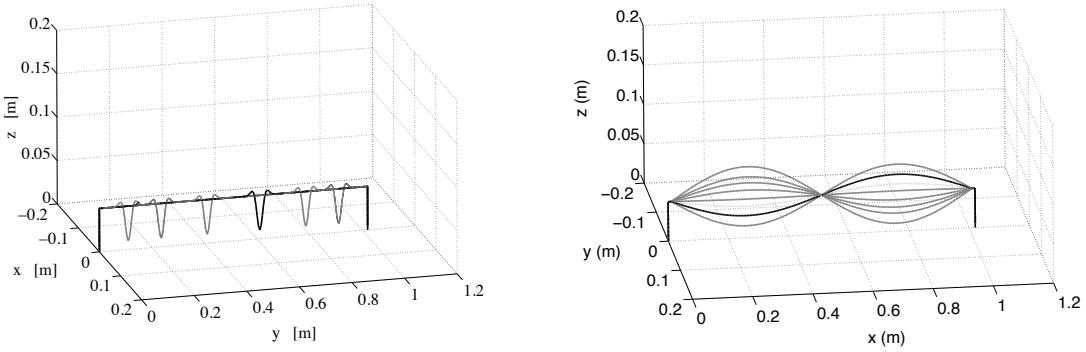

Figure 2. Examples of geometries resulting from the a local deformation (Figure (a)) and a global deformation (Figure (b)) of the axis of a thin wire.

In both cases, the wire is meshed into 224 segments. The incident field corresponds to a plane wave propagating in the direction $\theta = 45°$, $\phi = -90°$, and such that $\boldsymbol{E}^i$ lies in the plane of incidence, with $|\boldsymbol{E}^i| = 1$ V.m^{-1}. This field has a frequency f, which belongs to the range $[100; 300]$ MHz.

To clarify the notation, the statistical moments corresponding to the voltage induced at the port of S_w and S_h are indexed by the subscripts $_w$ and $_h$, respectively.

4.2. Complexity

At each frequency f, the statistical moments are computed by a trapezoidal quadrature rule which employs N evaluations of V_e to reach the target maximum relative error of 1 % for each of the integrals defining $\mathbb{E}[V_e]$, $\sigma[V_e]$ and $\kappa[V_e]$.

The resulting values of N, for the wires S_w and S_h, are plotted as a function of f in Figure 3. A single computation of the induced voltage amounts to 0.2 seconds. On average, the statistics are obtained using 59 and 133 calculations of V_e, for S_w and S_h respectively. For S_w, a peak of N=513 appears when $f = 202$

MHz, while for S_h, the maximum value $N = 257$ is attained at several frequencies, viz. around 130 MHz, between 177 MHz and 193 MHz and between 275 MHz and 300 MHz.

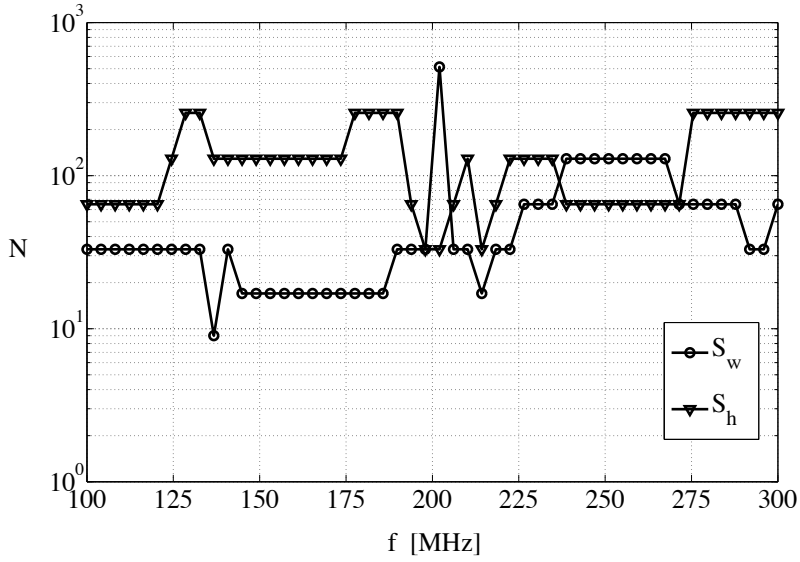

Figure 3. Complexity N to compute $\mu[V_e]$, $\sigma[V_e]$ and $\kappa[V_e]$ with a maximum relative error of 1%: wires S_w (circles) and S_h (triangles).

Overall, these performances are primarily dictated by the integral defining $\kappa[V_e]$, as it converges slower than $\sigma[V_e]$, which itself converges slower than $\mu[V_e]$. This argument is supported by Figure 4, where the relative error of the statistical moments is plotted versus the number N of function calls at $f = 300$ MHz.

4.3. Comparison of the standard deviations $\sigma[V_e]_w$ and $\sigma[V_e]_h$

The standard deviation depicted in Figure 5 shows that both $\sigma[V_e]_w$ and $\sigma[V_e]_h$ vary by three orders of magnitude in the range of frequencies considered. In general, $\sigma[V_e]_w$ is lower than $\sigma[V_e]_h$ except around 200 MHz, and for $f \geq 270$ MHz. The increase of $\sigma[V_e]$ in the vicinity of 200 MHz signals the presence of a resonance. The peak of $\sigma[V_e]_w$ appears at 202 MHz and is shifted with respect to the highest value of $\sigma[V_e]_h$, which occurs at 210 MHz. This shift can be explained by the difference of variations of the wires in terms of their random inputs: the random modifications of y_* in $[y_m, y_M]$ produce changes of the shape of S_w but do not modify its total length, whereas in the case of S_h both its shape and its total length vary as α assume different values in the interval $[-4, 4]$ cm.

Even though the geometrical deformation of S_w is localized on a narrow portion of the wire, relatively to the global deformation of S_h, it produces a more acute resonance peak. Moreover, the graph of $\sigma[V_e]_h$ reveals robust behavior for frequencies around 132 MHz and 284 MHz, where $\sigma[V_e]_h$ is minimal.

As highlighted in Section 3.2, the magnitude of $\sigma[V_e]$ indicates the extent of the spread of V_e around the mean $\mu[V_e]$. This spread can consist of a smooth distribution of V_e with a wide support, or, to the presence

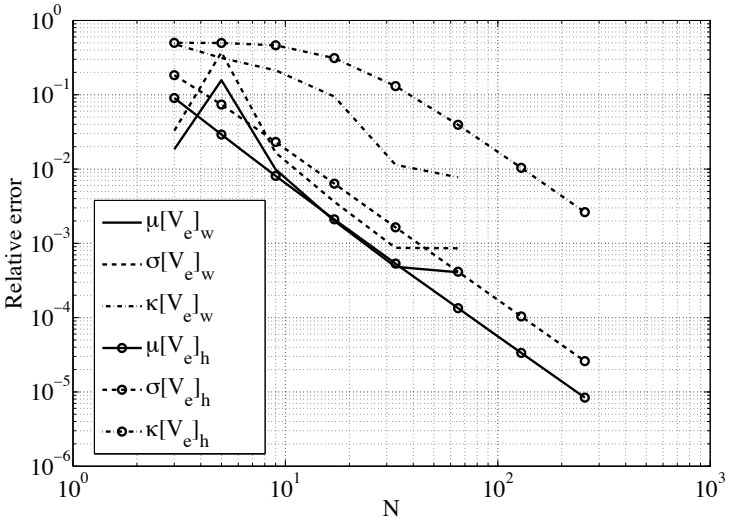

Figure 4. Relative error of the quadrature approximations of $\mu[V_e]$ (solid lines), $\sigma[V_e]$ (dashed lines) and $\kappa[V_e]$ (dash-dotted lines) at $f = 300$ MHz: wires S_w and S_h (circles).

of some extreme samples of V_e coexisting with a cluster of values around $\mu[V_e]$. The distinction between these two cases is possible through the analysis of the kurtosis.

4.4. Kurtosis

4.4.1. Wire S_w

The kurtosis $\kappa[V_e]_w$ of the voltage induced at the port of S_w is depicted in Figure 6, where its values can be compared to those of $\sigma[V_e]_w$. This figure reveals the limited risk of observing extreme samples, since $\kappa[V_e]_w$ remains below 3 for most of the frequencies. A sharp increase of $\kappa[V_e]_w$ appears around 202 MHz hereby revealing the increased statistical spread of the samples of V_e around this particular frequency. The highest effect of the resonance can hence be identified with a better resolution via the graph of $\kappa[V_e]_w$, comparatively to the graph of $\sigma[V_e]_w$.

The conclusions drawn from Figure 6 can be verified by assessing the actual distribution of V_e in the complex plane. To this end, 1000 deterministic values of V_e are computed at $f_{w,1}$=210 MHz and $f_{w,2}$=234 MHz, the resonance frequency $f_{w,r}$=202 MHz being discussed further in Section 4.4.3. These frequencies are chosen such that, although at $\sigma[V_e]_w(f_{w,1})$=206 mV is an order of magnitude larger than $\sigma[V_e]_w(f_{w,2})$=33 mV, the kurtosis $\kappa[V_e]_w(f_{w,1}) = 1.6$ and $\kappa[V_e]_w(f_{w,2}) = 2.4$ are comparable, with even $\kappa[V_e]_w(f_{w,1}) \leq \kappa[V_e]_w(f_{w,2})$. The 1000 deterministic samples are then normalized via Equation (6), and then plotted in the complex plane in Figure 7. The first normalized Chebychev circle, derived from Equation (5), is also plotted to mark a distance of $1\sigma[V_e]$ from $\mu[V_e]$.

The distribution of the samples confirms the comparable dispersion of V_e at both frequencies, with a slightly larger dispersion at 234 MHz.

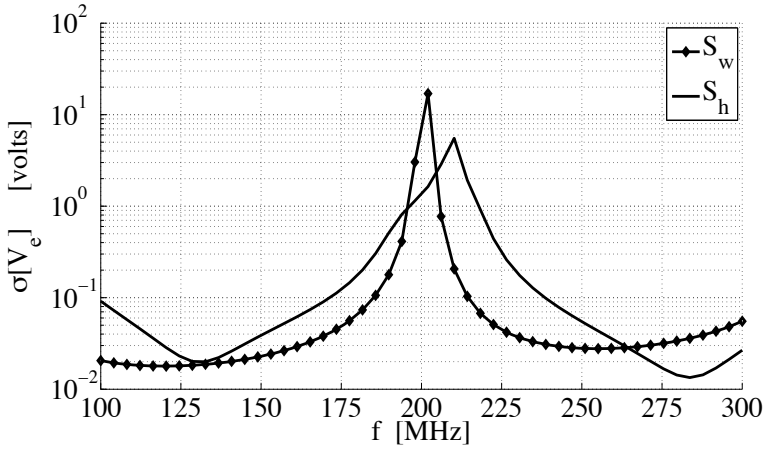

Figure 5. $\sigma\,[V_e]_w$ (circled line) and $\sigma\,[V_e]_h$ (dashed line) as a function of f.

4.4.2. Wire S_h

Concerning the voltage induced at the port of S_h, its kurtosis is represented in Figure 8, together with $\sigma[V_e]_h$. In comparison with Figure 6, the level of risk is higher even away from the resonance which occurs around $f_{h,r}$=210 MHz. The kurtosis provides a finer characterization of V_e than $\sigma\,[V_e]_h$ as it reveals the different types of sample distributions within a single resonance region. Frequencies can be identified where despite an important $\kappa[V_e]_h$, the value of $\sigma[V_e]_h$ remains relatively low, e.g. when $f \in [195, 205]$ MHz and $f \in [215, 225]$ MHz. In addition, a kurtosis larger than four is observed around the robust frequencies f=132 MHz and f=284 MHz.

All these observations are corroborated by the calculation of 1000 samples at both the frequencies $f_{h,1}$=202 MHz and $f_{h,2}$=284 MHz. The normalized samples are plotted together with the normalized Chebychev circles C_1 and C_2 in Figure 9. This plot confirms that regardless of the fact that $\sigma\,[V_e]_h$ is more than 100 times larger at $f_{h,1}$ than at $f_{h,2}$, the statistical spread of V_e is contrarily more pronounced at $f_{h,2}$, i.e. at $f_{h,1}$ all the samples of V_n are contained in C_2, while at $f_{h,2}$, samples such that $|V_n| > 2\sigma\,[V_e]_h$ are present.

A comparison between the evolution of the complexity N, shown in Figure 3, and the values of the kurtosis associated to S_h, plotted in Figure 8, shows that frequencies at which $\kappa[V_e]_h$ is important also correspond to frequencies where N is larger. This link can be understood by the definition of the kurtosis which measures the presence of extreme values taken by V_e, thereby indicating roughness of V_e in terms of the random input. This observation also stems from the use of a trapezoidal rule which depends on the smoothness of the integrand. As such this behavior differs from that of a Monte-Carlo quadrature rule, the convergence rate of which depends on the variance of its integrand [11].

4.4.3. Comparison of the resonances of S_w and S_h

Even though the resonances for the two wires appear at different frequencies, they can be mutually compared both with respect to $\sigma[V_e]$ and $\kappa[V_e]$. In terms of physical dispersion, the resonance of S_w gives rise to

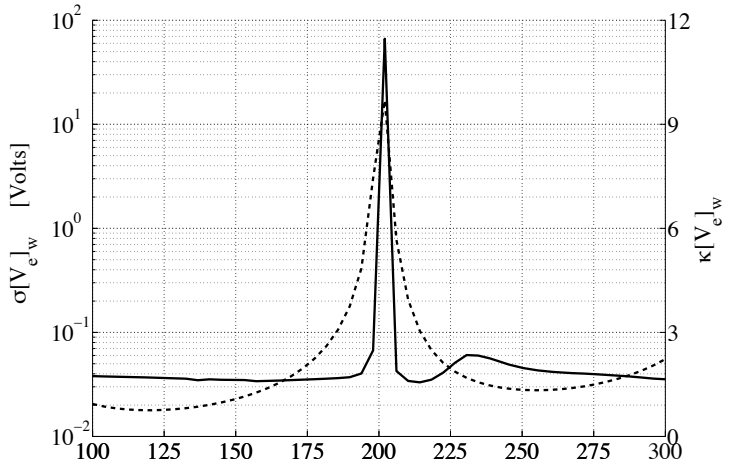

Figure 6. $\kappa[V_e]_w$ (solid line) and $\sigma[V_e]_w$ (dashed line) versus f.

$\sigma[V_e]_{w,max} = 17$ V, while the resonance of S_h leads to a peak value $\sigma[V_e]_{h,max} = 5$ V which is more than 3 times lower than $\sigma[V_e]_{w,max}$. This does not necessarily imply that the statistical dispersion of V_e will be three times as important for the resonance of S_w as for the resonance of S_h. On the contrary, the kurtosis is comparable at these two resonance situations, although larger for S_w, as revealed by $\kappa[V_e]_{w,max} = 11.4 \geq \kappa[V_e]_{h,max} = 9.1$. These features are endorsed by the sample distribution appearing in Figure 10, where again 1000 deterministic samples are computed for each of the resonance frequencies.

At resonances, the samples are distributed along a circular pattern both for S_w and S_h. All the samples associated with S_h are contained inside C_4, while for S_w the spread extends to the disk of radius 5.

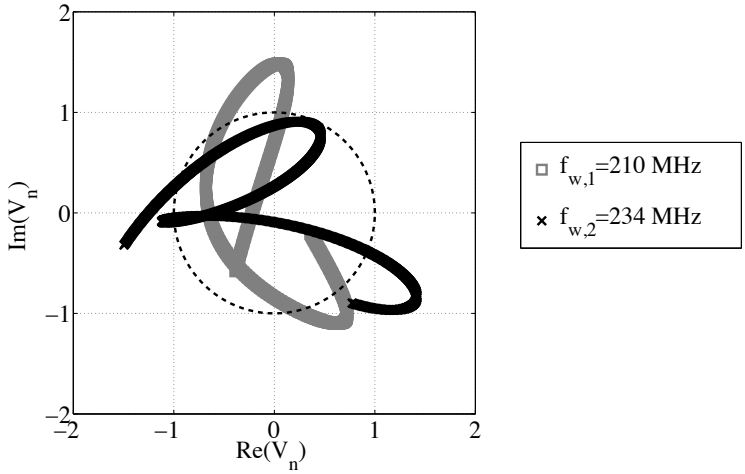

Figure 7. 1000 normalized samples V_n and Chebychev circle C_1.

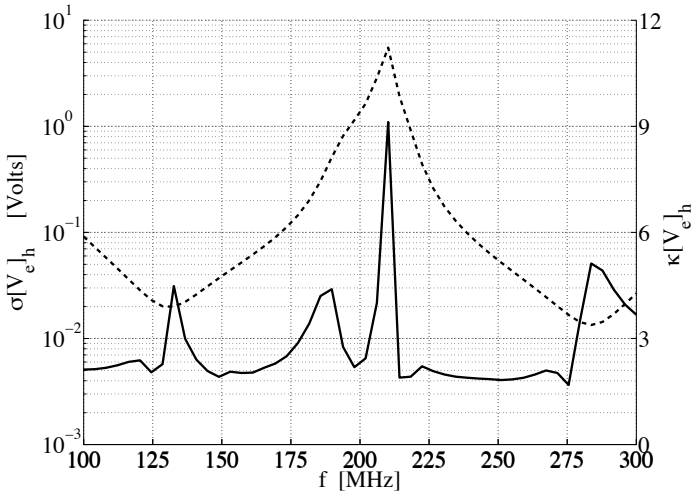

Figure 8. $\kappa[V_e]_h$ (solid line) and $\sigma[V_e]_h$ (dashed line) versus f.

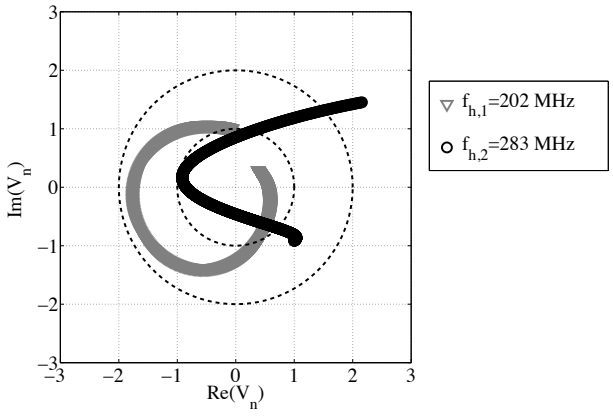

Figure 9. 1000 normalized samples V_n and Chebychev circles C_1 and C_2.

5. Conclusion

This paper has proposed a stochastic method of quantifying uncertainties affecting deterministic models of electromagnetic interactions. An efficient and accurate computation of the average, the variance and the kurtosis permits the assessment of the dispersion of the observable: the variance allows for the construction of confidence circles containing the majority of the values of the observable, whereas the kurtosis completes this information by indicating the likelihood of having extreme samples that lie far away from the mean.

The hierarchy in the numerical effort required to obtain these statistical moments has been highlighted by showing that accurate evaluation of higher order moments translates into a higher complexity. The results although shown in the case of a 1-D stochastic problem can be extended to higher dimensional problems, provided that efficient quadrature rules are employed.

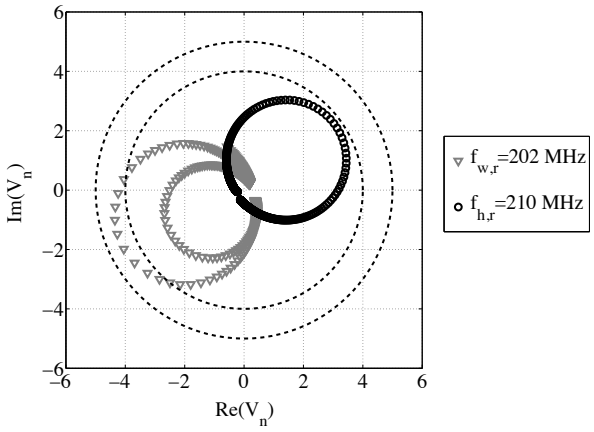

Figure 10. 1000 normalized samples V_n at resonances: $f_{w,r}$=202 MHz for S_w and $f_{h,r}$=210 MHz for S_h. Chebychev circles C_4 and C_5 (dashed lines).

This method has been employed to study two different types of thin-wire geometries that are nonetheless fundamental as they exemplify two generic geometrical parameterizations, viz. a harmonic Fourier model and a localized wavelet model. The global variations of the harmonic geometry lead to a large physical dispersion accounted for by a larger standard deviation about the mean. On the other hand, the localized wavelet perturbation provokes a larger resonance peak.

The analysis of the kurtosis has refined the information conveyed by the variance by revealing that a large value of the variance, equivalent to an important *physical* dispersion of the observable, could still correspond to a limited *statistical* dispersion revealed by a low fourth-order moment. The study of the kurtosis is therefore advisable to foretell situations where a seemingly limited physical variability of the voltage induced on an electronic device, dissimulates extreme values that can prove hazardous to the proper functioning of electronic equipment.

Acknowledgement

This work is funded by the Dutch Ministry of Economic Affairs, in the Innovation Research Program (IOP) number EMVT 04302.

References

[1] G.Andrieu, L. Kone, F. Bocquet, B. Demoulin, J.P. Parmantier, "Experimental validations of the equivalent cable bundle method", Proc. 18th International Zurich Symposium on Electromagnetic Compatibility, pp. 163-166, 2007

[2] D. Bellan, S. Pignari, "A probabilistic model for the response of an electrically short two-conductor transmission line driven by a random plane wave field", IEEE Trans. EMC., Vol. 43, pp. 130-139, 2001

[3] C. Charalambous, N. Menemenlis, "Statistical analysis of the received signal over multipath fading channels via generalization of shot-noise", Proc. IEEE International Conference on Communications, Vol. 7, pp. 2246-2250, 2001

[4] N.J. Champagne II, J.T. Williams, D.R. Wilton, "The Use of Curved Segments for Numerically Modeling Thin Wire Antennas and Scatterers" IEEE Trans. Antenna Propagation, Vol. 40, pp. 682-689, 1992

[5] C. Charalambous, N. Menemenlis, "Stochastic models for short-term multipath fading channels: chi-square and Ornstein-Uhlenbeck processes", Proc. 38th IEEE Conference on Decision and Control, Vol. 5, pp. 4959-4964, 1999

[6] X. Ferrieres, J.P. Parmantier, S. Bertuol, A.R. Ruddle, "Application of a hybrid finite difference/finite volume method to solve an automotive EMC problem" IEEE Trans. EMC., Vol. 46, pp. 624-634, 2004

[7] C. Fiachetti, F. Issac, B. Michielsen, A. Reineix, "Modelling field to equipment coupling in mode stirred chambers", Proc. IEEE International Symposium on EMC, Vol. 2, pp. 762-767, 2001

[8] C. Fiachetti, B. Michielsen, "Electromagnetic random field models for analysis of coupling inside mode tuned chambers", Electronics Letters, Vol. 39, pp. 1713-1714, 2003

[9] T. Gerstner, M. Griebel, "Numerical integration using sparse grids", Numerical Algorithms, Vol.18 (24), pp. 209-232, 1998

[10] D. Hill, "Plane wave integral representation for fields in reverberation chambers", IEEE Trans. EMC., Vol. 40, pp. 209-217, 1998

[11] A.R. Krommer, C.W. Ueberhuber, "Computational Integration", SIAM, 1998

[12] S. Mallat, "A Wavelet Tour of Signal Processing", Academic Press, 1999

[13] B. Mandelbrot, R. Hudson, "The (Mis)behaviour of Markets", Profile Business, 2004

[14] K.K. Mei, "On the integral equation of thin wire antennas", Trans. Antennas Propagation, Vol. AP-13, pp. 374-378, 1965

[15] B. Michielsen, "Analysis of the coupling of a deterministic plane wave to a stochastic twisted pair of wires", Zurich Symposium on EMC, pp. 439442, 2005

[16] B.L. Michielsen, "Probabilistic modelling of stochastic interactions between electromagnetic fields and systems", Comptes Rendus de l'Acadmie des sciences: Physique, Vol. 7, 543559, 2006

[17] G. Mrozynski, V. Schulz, H. Garbe, "A benchmark catalog for numerical field calculations with respect to EMC problems", Proc. IEEE International Symposium on Electromagnetic Compatibility, Vol. 1, pp. 497-502, 1999

[18] A. Papoulis, "Probability & Statistics", Prentice-Hall International, 1990

[19] J.P. Parmantier, I. Junqua, S. Bertuol, F. Issac, S. Guillet, S. Houhou, & R. Perraud, "Simplification Method for the Assessment of the EM Response of a Complex Cable Harness", Proc. 20th International Zurich Symposium on EMC, pp. 161-164, 2009

[20] O. Sy, J. Vaessen, B. Michielsen, M. van Beurden, A. Tijhuis, "Modelling the interaction of stochastic systems with electromagnetic fields" Proc. IEEE APS International Symposium, pp. 931-934, 2006

[21] O. Sy, J. Vaessen, M. van Beurden, A. Tijhiuis, B. Michielsen, "Probabilistic Study of the Coupling between Deterministic Electromagnetic Fields and a Stochastic Thin-Wire over a PEC Plane", Proc. International Conference on Electromagnetics in Advanced Applications ICEAA, pp. 637-640, 2007

[22] O. Sy, J. Vaessen, M. van Beurden, B. Michielsen, A. Tijhuis, A. Zwamborn, J. Groot, "Experimental validation of the stochastic model of a randomly fluctuating transmission-line", Proc. 38th European Microwave Conference EuMC, pp.833-836, 2008

[23] O. Sy, J. Vaessen, M. van Beurden, B. Michielsen, A. Tijhuis, "Probablistic characterization of resonant EM interactions with thin-wires: variance and kurtosis analysis", SCEE 2008 Book of Abstracts: Scientific Computing in Electrical Engineering, pp. 41-42, 2008

[24] O. Sy, M. van Beurden, B. Michielsen, "Analysis of stochastic resonances in electromagnetic couplings to transmission lines", Proc. 20th International Zurich Symposium on EMC, pp. 33-36, 2009

[25] J. Vaessen, O. Sy, M. van Beurden, A. Tijhuis, B. Michielsen, "Monte-Carlo method applied to a stochastically varying wire above a PEC ground plane", Proceedings EMC Europe Workshop, pp.1-5, 2007